Published in final edited form as:
Glia. 2005 January 15; 49(2): 245–258. doi:10.1002/glia.20110.

The Cytokine IL-1β Transiently Enhances $P2X_7$ Receptor Expression and Function in Human Astrocytes

LEONTINE NARCISSE[1], **ELIANA SCEMES**[2], **YONGMEI ZHAO**[1], **SUNHEE C. LEE**[1], and **CELIA F. BROSNAN**[1,2,*]

1*Department of Pathology, Albert Einstein College of Medicine, Bronx, New York*

2*Department of Neuroscience, Albert Einstein College of Medicine, Bronx, New York*

Abstract

Extracellular nucleotide di- and triphosphates such as ATP and ADP mediate their effects through purinergic P2 receptors belonging to either the metabotropic P2Y or the ionotropic P2X receptor family. The $P2X_7R$ is a unique member of the P2X family, which forms a pore in response to ligand stimulation, regulating cell permeability, cytokine release, and/or apoptosis. This receptor is also unique in that its affinity for the ligand benzoyl-benzoyl ATP (BzATP) is at least 10-fold greater than that of ATP. Primary human fetal astrocytes in culture express low-levels of $P2X_7R$ mRNA and protein, and BzATP induces only a slight influx in intracellular calcium $[Ca^{2+}]_i$, with little demonstrable effect on gene expression or pore formation in these cells. We now show that, following treatment with the proinflammatory cytokine IL-1β, BzATP induces a robust rise in $[Ca^{2+}]_i$ with agonist and antagonist profiles indicative of the $P2X_7R$. IL-1β also induced the formation of membrane pores as evidenced by the uptake of YO-PRO-1 (375 Da). Quantitative real-time PCR demonstrated transient upregulation of $P2X_7R$ mRNA in IL-1β-treated cells, while FACS analysis indicated a similar upregulation of $P2X_7R$ protein at the cell membrane. In multiple sclerosis lesions, immunoreactivity for the $P2X_7R$ was demonstrated on reactive astrocytes in autopsy brain tissues. In turn, $P2X_7R$ stimulation increased the production of IL-1-induced nitric oxide synthase activity by astrocytes in culture. These studies suggest that signaling via the $P2X_7R$ may modulate the astrocytic response to inflammation in the human central nervous system.

Keywords

human fetal astrocytes; P2 receptors; IL-1β; $P2X_7R$; calcium regulation; pore formation

INTRODUCTION

Extracellular nucleotides have emerged as a family of ligand-specific signaling molecules that participate in a wide range of cellular processes such as cell–cell communication, neurotransmission, smooth muscle contraction, cytokine processing and release, and platelet aggregation (reviewed in Burnstock and Williams, 2000). Cell surface receptors for extracellular tri- and di-nucleotides, such as ATP, belong to a family of P2 purinergic receptors broadly divided into metabotropic (P2Y) and ionotropic (P2X) classes. P2Y receptors ($P2YR_{1–14}$) are G-protein-coupled seven transmembrane receptors whereas P2X receptors ($P2XR_{1–7}$) are ligand-gated ion channels. Many cell types express multiple P2Y and/or P2X receptors.

*Correspondence to: Dr Celia F. Brosnan, Department of Pathology, Albert Einstein College of Medicine, 1300 Morris Park Avenue, Bronx, NY 10461. E-mail brosnan@aecom.yu.edu

The $P2X_7$ receptor subtype ($P2X_7R$) is an unusual member of the P2X family in that it is a nondesensitizing, nonselective cation channel with low sensitivity for ATP (mM range) in the presence of divalent cations (Di Virgilio, 1995; Falzoni et al., 1995; Surprenant et al., 1996). Replacing ATP with either the ATP analogue 2′,3′-O-(4-benzoyl-4-benzoyl)-ATP (BzATP) or the tetraacidic form ATP^{4-} (μM range), which has been postulated to be the physiologic agonist for $P2X_7R$ (Steinberg et al., 1987), triggers channel activity. An additional feature of the $P2X_7R$ is that repeated or prolonged application of agonists leads to the formation of a nonselective pore that is permeable to molecules with a molecular size of ≤900 Da (Rassendren et al., 1997). Initially it was thought that expression of the $P2X_7R$ was relatively restricted to cells of hematopoietic lineage, where it has been implicated in proliferation, giant cell formation, degranulation, cytolytic cell death and the ATP-dependent processing and release of cytokines such as interleukin-1β (IL-1β) (Laliberte et al., 1994; Di Virgilio, 1995; Falzoni et al., 1995; Surprenant et al., 1996; Chow et al., 1997; Rassendren et al., 1997; Virginio et al., 1999b; MacKenzie et al., 2001). More recently, however, the $P2X_7R$ has been found on diverse populations of cells, including Mueller cells (Pannicke et al., 2000), astrocytes (John et al., 2001; Panenka et al., 2001), Schwann cells (Colomar and Amedee, 2001), and neurons (Deuchars et al., 2001). In these cells, it has been implicated in the regulation of cytokine and chemokine expression, as well as in neuronal transmission, but pore formation and cytotoxicity has been less consistently observed.

In cultured human fetal astrocytes, we detected $P2X_7R$ expression by RT-PCR analysis, but ligands for this receptor failed to induce pore formation or significant change in cytosolic calcium levels. However, subsequent functional studies showed that the $P2X_7R$ agonist BzATP was able to enhance IL-1β-induced activation of the transcription factors AP-1 and NF-κB, as well as to regulate IL-1β-induced chemokine expression in astrocytes (John et al., 2001). Since cytokines have been shown to modulate expression and function of $P2X_7R$ in other cell types (Humphreys and Dubyak, 1998), we investigated whether a similar phenomenon occurs in astrocytes. The results support the conclusion that IL-1β leads to a transient change in the astrocytic expression of $P2X_7R$, resulting in increased responsiveness to specific $P2X_7R$ ligands in terms of calcium influx as well as the formation of a pore with limited permeability characteristics.

MATERIALS AND METHODS

Astrocyte Cultures and Cytokines

Enriched human fetal brain astrocyte cultures were established from second-trimester abortuses as described previously (Lee et al., 1992). All tissue collection was approved by the Institutional Clinical Review Committee. To obtain cultures essentially free of microglia, cells were plated at 4×10^7 cells per 10 ml medium per T75 cm^2 tissue culture flask. After 14 days in vitro, cultures were shaken to remove microglia and astrocytes subcultured by trypsinization for at least three passages. Culture purity was determined by immunohistochemistry for glial fibrillary acidic protein (GFAP) for astrocytes, (BioGenex, San Ramon, CA), microtubule-associated protein-2 for neurons, (Sigma, St. Louis, MO) and CD68 for microglia (DAKO, Carpinteria, CA). Microglia, which are nondividing cells in this system, do not survive this subculturing process and enriched astrocyte cultures typically contain <0.01% microglia contamination. Recombinant human IL-1β was a gift from the Biological Response Modifiers Program at the National Cancer Institute (Frederick, MD), or was purchased from Peprotech (Rocky Hill, NJ), and interferon-gamma (IFNγ) was purchased from Genzyme (Cambridge, MA). Cytokines were diluted in medium containing 2 mg/ml endotoxin-free human serum albumin (Baxter Healthcare Company, McGaw, IL). Astrocytes were activated with IL-1β at 10 ng/ml (equivalent to 20 U/ml). All other reagents were purchased from Sigma unless otherwise indicated.

Calcium Measurements

Human fetal astrocytes were plated on glass-bottomed microwell dishes (MatTek, Ashland, MA) and treated with IL-1β for the indicated time. Cells were loaded with 10 μM Fura-2 AM (Molecular Probes, Eugene, OR) for 45 min and changes in intracellular calcium determined as described previously (Scemes et al., 2000). In brief, Fura-2-loaded cells were viewed on a Zeiss (Oberkochen, Germany) epifluorescence microscope, and intracellular Ca^{2+} ($[Ca^{2+}]_i$) measured in loaded astrocytes bathed in phosphate-buffered saline (PBS), pH 7.4. The ratio of fura-2 fluorescence emitted at two excitation wavelengths (340 and 380 nm) was obtained by using a combined system of an optical filters wheel (Sutter Instruments, Burlingame, CA) and a shutter (Uniblitz, Rochester, NY) driven by an OEI computer through Metafluor software (Universal Imaging Media System; Downingtown, PA). The Fura-2 fluorescence ratio images were acquired with an intensified Quantex CCD camera (Photometrics; Tuscon, AZ) and analyzed with Metafluor Imaging System software (Universal Imaging). Fura-2 fluorescence ratio images were acquired continuously at a rate of 0.3 Hz before and after the addition of P2 receptor agonists. Intracellular calcium levels were obtained from regions of interest by measuring the ratio of fura-2 intensity emitted at 520 nm during excitation at 340 and 380 nm, using the calibration equation (Grynkiewicz et al., 1985). For inhibitor studies, intracellular calcium levels induced by the $P2X_7R$ agonist BzATP alone were compared with those obtained from cells pretreated for 30 min with 10 nM KN-62 or 45min with 1.4 μg/ml of either a neutralizing monoclonal antibody to $P2X_7R$ kindly supplied by Dr. Gary Buell (Serono Pharmaceutical Research Institute, Geneva, Switzerland, (Buell et al., 1998)) or a mouse monoclonal isotype control that recognized human neurofilament protein of 68 kD (NF68, kindly supplied by our colleague Dr P. Davies, AECOM). Data shown represent pooled data from three to four experiments and three to four different brains.

RT-PCR

Total RNA was harvested from astrocytes using Trizol reagent (Invitrogen, Carlsbad, Ca) before and after treatment with IL-1β at 10 ng/ml for the indicated times. In some cases, cells were resuspended in RNAlater (Ambion, Austin, TX) and stored at −70°C before RNA extraction. cDNA transcribed from 1 μg RNA for each time point was used for PCR (35 cycles, Superscript One-Step RT-PCR, Invitrogen). Primers for human $P2X_7R$ were from Pannicke et al. (2000), primers for $P2X_5R$ were from Berchtold et al. (1999), and primers for $P2X_2R$ and $P2X_4R$ from Nakamura et al. (2000). Control primers for the human porphyrobilinogen deaminase gene were from Mensink et al. (1998). Photography and densitometric analysis of resulting PCR products was performed using a ChemiImager 4000 system and ChemiImager v5.5 software (Alpha Innotech, San Leandro, CA). Transcripts were cloned and sequenced to confirm target amplification.

Real-time quantitative PCR (qPCR) was performed on cDNA transcribed from 4 μg RNA using the Roche LightCycler. Serial dilutions of resting astrocyte cDNA were used to generate a standard curve for the PBGD control gene (primers from Faneyte et al., 2001) and $P2X_7$ (primers from O'Reilly et al., 2001). Triplicate samples were analyzed for each time point, and the data ratiometrically corrected using results obtained for PBGD. The resulting values were normalized such that the 0-h time point was equal to one, with data from other time points expressed as the fold-induction over the resting state. For both types of RT-PCR, experiments were repeated using cDNA from three different brains, and representative data shown.

YO-PRO-1 Uptake and Pore Formation

Human fetal astrocytes were plated in 24-well plates and treated with IL-1β as indicated. All pore formation assays were performed at 37°C, using divalent-free solutions to facilitate pore activity. Where KN-62 inhibition was examined, cells were preincubated with 10 nM KN-62 for 30 min before assessment of YO-PRO-1 uptake. The plates were washed and then given

PBS containing 10 μM YO-PRO-1 and 10 μg/ml Hoescht 33342 (Molecular Probes) with or without 100 μM BzATP. After a 10-min loading period the cells were visualized on an Olympus IX70 microscope (Melville, NY) with a 40× 0.6 optic. Images were collected with a Photometrics cooled CCD camera with a KAF 1400 chip using I.P. Lab Spectrum (Scanalytics, Fairfax, VA) on a Power Macintosh. For these experiments, cells from four different brains were analyzed and representative images shown.

YO-PRO-1 emission was quantified in astrocytes plated in 96-well black-walled, clear bottom plates (Corning International, Corning, NY) using a Spectra-Max Gemini spectrofluorimeter running SOFTmax-PRO 3.0 (Molecular Devices, Sunnyvale, CA) with excitation at 491 nm, and emission at 509 nm. Fluorescence was assayed at times indicated after BzATP addition and expressed as a percentage of background mean fluorescence intensity (MFI). Propidium iodide (PI) uptake was similarly measured, using 10 μM PI and excitation at 535 nm, emission at 617 nm. Lactate dehydrogenase secretion was measured in supernatants using the Lactate Dehydrogenase LD-L kit (Sigma Diagnostics) according to the manufacturer's instructions. Astrocytes from three different brains were used for the spectrofluorimetry experiments.

Cell Fractionation and Western Blotting

For preparation of membrane fractions, the procedure detailed by Ramirez and Kunze (2002) was adopted. In brief, cells were washed twice with ice-cold PBS, scraped into 1 ml cold PBS and pelleted at 1,000*g* (3,000 rpm) for 5 min. Cells were lysed by resuspension in ice-cold hypotonic lysis buffer (10 mM HEPES, pH 7.9, 10 mM KCl, 1.5mM $MgCl_2$, 50 mM NaF 1 mM Na_3VO_4, 1 μM PMSF plus a protease inhibitor cocktail), incubated on ice for 15 min, sonicated and spun at 1,000*g* for 10 min at 4°. Nuclei and unbroken cells were discarded, and the supernatant spun at 10,000*g* for 10 min at 4° to remove mitochondria, after which the supernatant was spun at 50,000*g* for 1 h at 4°. The membrane pellet was washed once with lysis buffer and recentrifuged to remove cytosolic contaminants. The final membrane pellet was solubilized in iosotonic lysis buffer containing 1% Triton X-100. After incubation on ice for 30 min, the insoluble debris was removed by centrifugation at 20,000*g* for 10 min. Protein samples were separated on 7.5% polyacrylamide SDS gels and transferred to polyvinylidene difluoride (PVDF) membranes, blocked with 5% milk in PBS-0.1% Tween-20 for 1 h and incubated overnight with primary antibody (anti-$P2X_7$, 1:2000, BD-Pharmingen, Franklin Lakes, NJ), or with antibody that had been adsorbed with the specific peptide (1:1 molar ratio, v/v for 1 h at RT as per the manufacturers instructions). Membranes were washed with PBS-Tween, incubated for 1 h with goat anti-rabbit horseradish peroxidase (HPO)-linked secondary antibody (1:2,000; Santa Cruz) in blocking buffer. Blots were washed and developed using the ECL-PLUS kit (Amersham). Equivalence of loading was determined from Coomassie blue-stained gels.

Immunohistochemistry

Human fetal astrocytes were plated on glass-bottomed microwell dishes (MatTek) and treated with IL-1β for the indicated times. Cells were fixed either with 4% freshly-prepared paraformaldehyde in PBS for 20 min on ice or in 100% methanol for 20 min on ice. No difference was noted in the staining pattern following the two fixation procedures, and all subsequent experiments used paraformaldehyde. Following three washes with PBS, cells were permeabilized with PBS containing 10% normal goat serum (NGS) and 0.3% Triton for 10 min on ice, followed by three washes with PBS. Culture dishes were blocked with 10% NGS in PBS for 1 h and then incubated in an affinity-purified rabbit anti-$P2X_7R$ antibody (BD Pharmingen) diluted 1:100 in 5% milk overnight at 4°. Cells were then washed and incubated with goat anti-rabbit Alexa 488 (Molecular Probes) diluted 1:100 in PBS containing 1.5% bovine serum albumin (BSA) and 0.1% Triton. Cultures were washed in PBS and stained with rhodamine phalloidin (Molecular Probes) at 1:20 for 10 min to visualize actin filaments, nuclei

were visualized with 4′,6-diamidino-2-phenylindole, dihydrochloride (DAPI, Molecular Probes), and cells covered with aqueous mounting medium (Biomeda, Foster City, CA). Control cultures were prepared by omitting the primary antibody. In some experiments, the fluorophores were reversed. Cells were visualized on an Olympus IX70 microscope with a 60× N.A. 1.4 infinity-corrected optic. Images were collected with a 60× objective using a Photometrics cooled CCD camera with a KAF 1400 chip using I.P. Lab Spectrum on a Power Macintosh. For these experiments, cells from at least three different brains were examined.

For analysis of the inducible form of nitric oxide synthase (NOS2), astrocytes were plated on 8-well chambered slides (Nalge Nunc International, Naperville, IL). Cells were treated with a combination of IL-1β, IFNγ (both at 10 ng/ml) with and without BzATP 100 μM BzATP and 10 nM KN-62 for the time indicated. Inducible nitric oxide synthase (NOS2) was visualized using a rabbit polyclonal antibody (Santa Cruz Biotechnology), followed by a peroxidase-conjugated goat anti-rabbit antibody (Vector Laboratories, Burlingame, CA). Cells were counterstained with hematoxylin and mounted. Brightfield images were visualized and photographed on a Leitz DM IRB inverted microscope using a 20× Hoffman modulation contrast optic (Modulation Optics, Greenvale, NY) and an Olympus DP12 system. Astrocytes from three different brains were visualized and representative data shown.

FACS Analysis

Preparation of astrocytes for fluorescence-activated cell sorting (FACS) analysis was performed essentially as described (Lee et al., 1995), and the protocol for $P2X_7R$ expression was according to Gudipaty et al. (2001), using the MAb (isotype IgG2b) to $P2X_7R$ (Buell et al., 1998) or a mouse monoclonal isotype control (Sigma, clone MOPC 141, cat. no. M8894, Sigma). The receptor was subsequently visualized using a goat anti-mouse IgG2b antibody conjugated to phycoerythrin. Data for cell staining (10,000 cells per sample) were acquired using a FACSCalibur and results analyzed using WinMDI CellQuest software (Becton Dickinson, San Diego, CA).

Immunohistochemical Analysis of Autopsy Tissues

In this study, 4-μm-thick, paraffin-embedded, formalin-fixed brain tissues were obtained from Dr. Cedric S. Raine (Albert Einstein College of Medicine) or from the Clinical Neuropathology Service of the Albert Einstein College of Medicine. All tissue collection was approved by the Institutional Clinical Review Committee. Analysis of pathology was performed on hematoxylin and eosin (H&E)-stained slides and lesion activity assessed according to established criteria (Raine, 1997). A total of 7 MS cases, containing 11 lesions that expressed characteristics of acute (n = 4), chronic active (n = 4) and chronic silent (n = 3) pathology were examined. In addition, three brains from individuals that died with no known central nervous system involvement were studied as controls. Deparaffinized sections were boiled in PBS for 10 min for antigen retrieval. Sections were incubated with 3% H_2O_2 for 30 min, and blocked with 10% normal goat serum for 1 h. Rabbit antihuman $P2X_7R$ (BD-Pharmingen) was used at a concentration of 1:200 and incubated overnight at 4°C. The secondary antibody was biotinylated anti-rabbit antibody used at a concentration of 1:200. For identification of astrocytes, sections were stained with a polyclonal antibody specific for GFAP (1:250, BioGenex, San Ramon, CA). Control slides were prepared using either omission of the primary antibody, or were incubated in parallel with the rabbit anti-$P2X_7R$ antibody that had been adsorbed with specific peptide (1:1 molar ratio, v/v for 1 h at RT as per manufacturer's instructions). In all cases, parallel sections were developed using both the ABC method (Vectastain; Vector Laboratories), and the Tyramide Signal Amplification Technology (Molecular Probes). Diaminobenzidine (DAB, brown) was used as the chromogen according to standard protocols.

Nitric Oxide Measurement

Astrocytes were treated with both IL-1β (10 ng/ml) and interferon-γ (IFNγ, 10 ng/ml) for the time indicated. In addition to the above cytokines, cells were treated with 100 μM ADP, ATP, UTP, or various doses of BzATP with or without a 30-min pretreatment with 10 nM KN-62 as indicated. Nitrite was measured in cell supernatants collected, after indicated treatment using the Griess reagent as described previously (Lee et al., 1993). Data shown represent data pooled from three independent experiments and three different brains.

Statistical Analysis

Prism 4.0 was used for all statistical analysis (GraphPad Software, San Diego, CA). All pEC50 analysis was performed using nonlinear regression with a variable slope curve fit. Where applicable, results are presented as mean ±SD or mean ±SEM as stated in text. Statistical analysis was performed using either Student's *t*-test with a 95% confidence or ANOVA followed by the indicated posttest. P-values are shown for each analysis.

RESULTS

IL-1β Increases Astrocytic Intracellular Calcium in Response to BzATP

We and others have shown previously that ATP in the μM range induces intracellular calcium transients in astrocytes due to activation of the metabotropic $P2Y_1$ receptor subtype (see, e.g., Liu et al., 2000). The pharmacological characteristics of the $P2X_7R$ differ from P2Y receptors in showing only a low affinity for ATP (mM range) and a relative resistance to desensitization (for review, see Burnstock and Williams, 2000). To determine whether the $P2X_7R$ detected previously by RT-PCR analysis in cultured human fetal astrocytes (John et al., 2001) was functionally present on the cell surface, intracellular calcium levels were monitored in response to the $P2X_7R$ ligand BzATP in control cells and IL-1β-treated astrocytes. An example of mean intracellular calcium levels in control cells and in astrocytes 24 h post-activation with IL-1β is shown in Figure 1A. In untreated cells, 100 μM BzATP induced a modest calcium influx (peak influx over baseline 80 ± 21 nM). As is typical of BzATP stimulation, this elevation in $[Ca^{2+}]_i$ persisted until the agonist was washed out. By contrast, IL-1β activation markedly increased the amplitude of the intracellular calcium rise elicited by BzATP (peak influx over baseline 170 ± 19 nM), both for the initial component of the response, as well as for the more sustained rise in $[Ca^{2+}]_i$. The magnitude of this increased calcium response to BzATP in IL-1β-treated astrocytes was dose dependent (Fig. 1B; 33 ± 1.8, 140 ± 21 and 170 ± 19 nM influx for 1, 10 and 100 μM BzATP, respectively, $P < 0.01$) and also reflected an increase in the number of cells responding to agonist following cytokine activation (Fig. 1C; 21%, 82%, and 100% for 1, 10, and 100 μM BzATP, respectively). Thus IL-1β increased both the magnitude of response in individual cells, as well as the number of cells capable of responding. The measured pEC50 of this response was 5.42 ± 0.2, similar to that observed for the recombinant $P2X_7R$ (5.33 ± 0.02 (Bianchi et al., 1999).

To characterize further the response to BzATP in cytokine-activated astrocytes, we stimulated the cells in the presence of various inhibitors of the $P2X_7R$ (Fig. 1D). Consistent with a role for a P2X receptor, in the absence of extracellular Ca^{2+} a sharp reduction in the amplitude of agonist-induced Ca^{2+} transients was observed (25.6 ± 9.9% of BzATP alone). In support of the role for the $P2X_7R$ in this response, the $P2X_7R$ antagonist KN-62 (10 nM) decreased the action of BzATP (20.8 ± 2.2% of the response to BzATP) at a concentration shown to selectively inhibit human $P2X_7R$ without affecting the activity of CAM kinase II, or $P2X_4$ (Gargett and Wiley, 1997;Humphreys et al., 1998;Jones et al., 2000). Furthermore, a blocking monoclonal antibody to $P2X_7R$ strongly dampened the BzATP- induced Ca^{2+} response to 14.5 ± 1.3% of BzATP alone (Buell et al., 1998), whereas an irrelevant antibody had no effect (106.7

± 13.2). The antibody has no reactivity to $P2X_1$ or $P2X_4$. All inhibitors were significantly different from the response to unopposed BzATP ($P < 0.001$) except the irrelevant antibody.

Astrocytic Formation of Membrane Pores Is Enhanced by IL-1β

A characteristic feature of the $P2X_7R$ in hematopoietic cells is the formation of a large transmembrane pore permeable to molecules < 900 Da in the presence of prolonged or repeated application of agonist (Steinberg et al., 1987; Di Virgilio, 1995; Surprenant et al., 1996). More recently, formation of similar pores has been demonstrated upon activation of $P2X_2$, $P2X_4$, and $P2X_5$ receptors (Virginio et al., 1999b; Bo et al., 2003). However, transition to pore formation for $P2X_7R$ has not been so consistently demonstrated in other cell types, particularly in cells of human origin (see, e.g., Pannicke et al., 2000). In our previous studies of the effect of ATP on human fetal astrocytes in culture, we failed to detect pore formation in these cells (Liu et al., 2000). To determine whether this response was altered by cytokine activation, cells were treated with IL-1β and alterations in membrane permeability determined using the fluorescent dye YO-PRO-1 (M_r = 375 Da). This dye binds to DNA and thus in cells permeabilized by BzATP will selectively localize to the nucleus. As expected, untreated astrocytes took up little of the dye in the presence of 100 μM BzATP (Fig. 2A, bottom row). By contrast, 24 h IL-1β treatment prior to the addition of BzATP increased both the number of fluorescently labeled cells, as well as the intensity of the nuclear staining. This observed increase in cell permeability could be inhibited by pretreatment with 10 nM KN-62, which has been demonstrated to block YOPRO-1 uptake initiated by prolonged activation of $P2X_7R$ (Wiley et al., 1998). Addition of divalent ions to the assay buffer markedly decreased dye uptake with the order $Zn^{2+} > Mg^{2+} > Ca^{2+}$ (10 μM, 500 μM and 1 mM, respectively), also suggestive of a $P2X_7$-dependent phenomenon (data not shown). In all samples, little cell loss or cytolysis was observed, as demonstrated by imaging the uptake of Hoescht, a cell-permeant dye that stains nucleic acid (Fig. 2A, middle row). Despite their exposure to 100 μM BzATP for 10 min, with or without KN-62 pretreatment, the astrocytes in all groups appeared to be of similarly confluent density, demonstrating an absence of cell detachment or lysis.

Increases in YO-PRO-1 fluorescence were also evaluated quantitatively by spectrofluorimetry. In response to 100 μM BzATP, resting and IL-1β-treated astrocytes displayed a progressive increase in dye up-take that was statistically significantly greater in cytokine-treated cells (Fig. 2B; $P < 0.001$). In IL-1β-activated astrocytes, dye uptake was dose-dependent (Fig. 3C; 27.6 ± 2.3, 38.9 ± 2.8, 43.5 ± 3.7, and 61.9 ± 4.3% increase in MFI over background for 10, 100, 200, and 300 μM BzATP at 10 min after nucleotide and dye exposure, $P < 0.001$). KN-62 pretreatment quantitatively blocked YO-PRO-1 uptake caused by addition of 100, 200, or 300μM BzATP decreasing %MFI over baseline to 15.0 ± 2.9, 20.5 ± 3.3, and 29.9 ± 2.8, respectively ($P < 0.01$ for 100 and 200 μM, $P < 0.001$ for 300 μM). Similar experiments performed with propidium iodide (PI, M_r = 415Da) did not demonstrate dye uptake in either treated or untreated astrocytes, suggesting a limitation in the nature of the developed pore in these cells (data not shown, see also discussion). Analyses of cell media collected over 2 h after BzATP addition was negative for the presence of lactic dehydrogenase, further indicating that BzATP does not induce an immediate cytolytic response in either control or IL-1β-activated astrocytes (data not shown).

IL-1β Increases Astrocytic Expression of $P2X_7R$ mRNA, and Protein Translocation to the Membrane

To determine whether the functional increase in $P2X_7R$ activity that we detected by the above methods in IL-1β-activated cells reflected induction of the $P2X_7R$ gene, and/or a redistribution of $P2X_7R$ protein in the cell, we used a combination of RT-PCR analysis, immunohistochemistry, FACS analysis, and Western blotting. mRNA was prepared from control and IL-1β-treated astrocytes and RT-PCR analysis performed using primers for human

$P2X_2$, $P2X_4$, $P2X_5$, and $P2X_7$ receptors, as well as a control gene, porphobilinogen deaminase (PBGD) (Fig. 3A). Resting astrocytes expressed RT-PCR product for $P2X_4$, $P2X_5$, and $P2X_7$ but no $P2X_2$ receptors. Following treatment with IL-1β, densitometric analysis showed a 3-fold increase in $P2X_7R$ message levels over baseline at 6 h and a 2-fold increase at 24 h, with mRNA levels returning to resting values by 48 h. A slight increase in $P2X_4R$ mRNA was also noted, whereas levels of $P2X_5R$ and PBGD remained constant. More sensitive qPCR analysis of this expression confirmed a transient upregulation, with upregulation peaking 4 h after treatment with a return to baseline by 24 h posttreatment (Fig. 3B, 31.1 ± 4.8 at 4 h, $P < 0.01$).

We then assessed $P2X_7R$ expression in control and IL-1β-treated astrocytes using immunohistochemistry with a polyclonal antibody directed against an epitope in the C-terminus. Cells were counterstained for actin using rhodamine-phalloidin, and nuclei identified with DAPI. In resting astrocytes, a prominent signal for $P2X_7R$ was detected in a perinuclear region, consistent with localization in the Golgi region (Fig. 4A). Discrete punctate staining was also detected rarely at the cell membrane (Fig. 4B). Following activation with IL-1β for 24 h, astrocytes in culture undergo a shape change that results in an increase in the number of cell processes and a loss of the actin-based cytoskeleton. A typical IL-1β-treated astrocyte is shown in Figure 4C. In cells that undergo this shape change, immunoreactivity for $P2X_7R$ was less evident in the Golgi region, but cell processes were extensively decorated with punctate immunoreactivity for $P2X_7R$ (Fig. 4D).

To assess changes more accurately in cell surface expression of the $P2X_7R$, we used a monoclonal antibody directed against an extracellular epitope of the $P2X_7R$ with a nonpermeabilization procedure for FACS analysis. Resting astrocytes in culture showed little evidence of cell surface expression of $P2X_7R$, consistent with the calcium measurements (Fig. 4E, 13% positive). However, a striking increase in cell surface expression was noted 24 h following activation with IL-1β that involved essentially all of the gated cell population. This had diminished to 46.5% positive cells by 48 h, but was still considerably elevated over that found at the 0-h time point. In contrast, parallel cultures that were stained with an irrelevant isotype-matched antibody failed to show any change in staining pattern following activation with IL-1β (10.5%, 11.0%, and 11.2% for 0, 24, and 48 h, respectively).

To assess further membrane expression of these proteins, cell homogenates obtained from both the SHSY5Y neuroblastoma cell line and control and IL-1β-treated astrocytes were prepared and postnuclear supernatants centrifuged to obtain a membrane fraction free of nuclear components. This strategy was adopted because immunoreactivity for $P2X_7R$ has been detected in the nuclei of some cells (Atkinson et al., 2002). In these blots, a clear band at ~78 kD was observed at 24 h, consistent with the major band found in the membrane fraction derived from the SH-SY5Y neuroblastomas that have been shown to express functional $P2X_7R$ in vitro (Per Larsson et al., 2002). In addition, a band at ~50 kD was elevated in the membrane fraction following 24-h treatment with IL-1β, that had substantially diminished by 72 h (Fig. 4F). Both bands were lost following adsorption of the antibody with specific peptide (data not shown). These data support the conclusion that treatment with IL-1β leads to a transient increase in the 50-kD and 78-kD isoforms of the $P2X_7R$ that are present at the cell membrane.

Immunoreactivity for $P2X_7R$ in Multiple Sclerosis Lesions

The observation that treatment with IL-1β resulted in increased expression of the $P2X_7R$ raised the question as to whether reactive astrocytes in the inflamed CNS also expressed detectable levels of $P2X_7R$ in vivo. Therefore, we immunostained multiple sclerosis lesions with the polyclonal anti-$P2X_7R$ antibody to test this hypothesis (Fig. 5). In white matter, lesioned areas of the brain showed prominent reactivity for the $P2X_7R$ (5A, perivascular inflammatory cuffs marked with an asterisk). Cells within the perivascular infiltrates (Fig. 5B,C, arrowheads),

endothelial cells (Fig. 5C, arrow), as well as hypertrophic astrocytes (Fig. 5A,B,D, arrows) located at the border of a chronic-active lesion showed $P2X_7R$ immunoreactivity. The identification of these cells as hypertrophic astrocytes was further supported by staining of parallel sections with the astrocyte-specific intermediate filament GFAP (inset, Fig. 5B). Neurons also stained strongly for $P2X_7R$ (5E). Specificity of the $P2X_7R$ staining was determined by incubating serial sections with antibody that had been adsorbed with specific peptide (Fig. 5F,G). In noninflamed areas of the CNS, neurons showed prominent staining for the $P2X_7R$ whereas the adjacent noninflamed white matter showed only a low-level of reactivity (Fig. 5H). Although a detailed analysis of $P2X_7R$ immunoreactivity with respect to MS lesion subtype was not the objective of the present study, $P2X_7R$+ reactive astrocytes could be identified in all types of MS lesions, particularly following TSA processing. In contrast, in normal CNS tissues, only subpopulations of neurons were readily identifiable as $P2X_7R^+$ cells, comparable to that shown for noninvolved tissues from MS brains (Fig. 5H).

BzATP Enhances NO Production Induced by IL-1β/IFNγ

It has previously been demonstrated that activation of astrocytes with cytokines upregulates their expression of inducible nitric oxide synthase (NOS2) and production of nitric oxide (NO) (Lee et al., 1993). While IL-1β alone can induce NO production, co-treatment with IFNγ greatly enhances this response. Extracellular nucleotides have been shown to increase IL-1β activation of the transcription factors AP-1 and NF-κB, which would be expected to enhance activation of NOS2 (Ferrari et al., 1997; John et al., 2001). Indeed, blockade of purinergic receptors with oATP has been shown to decrease macrophage production of NO in response to lipopolysaccharide (Hu et al., 1998), and more recently it has been demonstrated that BzATP can enhance production of NO induced by IFN-γ in a microglial cell line (Gendron et al., 2003b). Given the above effects of BzATP, we examined the impact of $P2X_7R$ activation on NOS2 induction (Fig. 6). Astrocytes were treated with IL-1β/IFNγ in the presence or absence of BzATP for 72 h, and then immunostained for NOS2. This time point was chosen based on previous data (Lee et al., 1993). Untreated astrocytes showed little to no NOS2 immunoreactivity (Fig. 6A), while IL-1β/IFNγ co-treatment induced shape change and NOS2 expression in astrocytes, with more stellate astrocytes staining more intensely (Fig. 6B, arrows). In the context of cytokine activation BzATP greatly enhanced immunoreactivity for NOS2 (Fig. 6C, arrows), although BzATP alone did not induce NOS2 immunoreactivity (data not shown). The effect of BzATP co-treatment on NOS2 induction could be abolished by pretreatment with KN-62 (Fig. 6D).

More quantitative analysis of NOS2 activity was performed by measurement of astrocytic nitrite production. As shown in Figure 6E, addition of BzATP to the IL-1β/IFNγ activation stimulus enhanced astrocytic nitrite production (27.7 ± 0.8 and 53.4 ± 2.2 μM nitrite for I/I and BzATP + I/I, respectively, $P < 0.01$). This enhanced response was dose-dependent, increasing production to 45.0 ± 5.7, 53.8 ± 1.0 and 54.9 ± 5.0μM nitrite for 10, 100, and 300 μM BzATP (Fig. 6F, $P < 0.05$, 0.01, and 0.001, respectively). By contrast, the various P2Y agonists tested showed no significant effect on nitrite levels, except ADP, which decreased nitrite production to 21.7 ± 1.0 μM, $P < 0.05$ (Fig. 6E). Treatment with BzATP alone had no effect on NO production (data not shown). While ATP is also a $P2X_7R$ agonist, the concentration used here (100 μM) would not be expected to activate $P2X_7R$s. Blockade of BzATP by 10 nM KN-62 was assessed at the same doses of BzATP (Fig. 6G). In this experiment, co-treatment of I/I-activated cells with BzATP resulted in values of 111.3 ± 3.7, 138 ± 8, and 171.3 ± 12% of the I/I control for 10, 100, and 300 μM BzATP. Pretreatment of cells with 10 nM KN-62 significantly reduced these levels to give values of 101.5 ±6, 104.3 ± 6.6 and 136.0 ± 10.0% of the I/I control for 10, 100, and 300 μM BzATP (Fig. 6G; $P < 0.05$ and 0.01, respectively).

DISCUSSION

In this study, we have shown that the expression of the $P2X_7R$ can be transiently upregulated in human fetal astrocytes in culture by the cytokine IL-1β. Increased expression was determined using a combination of RT-PCR for mRNA analysis in conjunction with FACS analysis for protein expression. Functional studies included the demonstration of an enhanced and prolonged calcium influx in response to ligand activation that was dependent on extracellular Ca^{2+} ions, and which was blocked by the $P2X_7R$ antagonist KN-62 and a neutralizing antibody to $P2X_7R$. Treatment with IL-1 also upregulated BzATP-induced increased permeability to the large organic molecule YO-PRO-1. That these data may have relevance to astrocytic function in the inflamed CNS was supported by the observation that $P2X_7R$ activation modulated IL-1β-expression of the inducible form of nitric oxide synthase, and that staining for $P2X_7R$ could be detected on reactive astrocytes in an inflammatory disease of the CNS where IL-1β has been shown to be upregulated (Liu et al., 2001).

In differentiated cells of the hematopoietic lineage, the $P2X_7R$ functions as an ATP-gated cation channel, but also demonstrates the formation of nonselective pores following prolonged stimulation. The processing and release of cytokines such as IL-1 and IL-18, as well as the initiation of cell death, have been found to be dependent on the pore forming ability of this receptor and the sustained increase in $[Ca^{2+}]_i$ (Laliberte et al., 1994; Di Virgilio, 1995; Falzoni et al., 1995; Surprenant et al., 1996; MacKenzie et al., 2001; Gudipaty et al., 2003), a conclusion that has been further supported by studies in mice in which the gene for the $P2X_7R$ has been inactivated (Solle et al., 2001).

Structure—function studies have shown that only a small portion of the cytosolic region is required for channel activity, whereas pore formation resides within the long C-terminal tail (Surprenant et al., 1996; Rassendren et al., 1997; Gu et al., 2001; Smart et al., 2003). Recently, it has been demonstrated that the C-terminus interacts with at least 11 intracellular proteins, including several cytoskeletal and signaling molecules, that may prove vital for proper channel and/or pore formation and function (Kim et al., 2001).

In an analysis of cytokine-differentiated THP-1 cells and blood-derived monocytes, Dubyak and colleagues suggested that the increased pore forming capacity of these cells reflected, at least in part, an increased density of $P2X_7Rs$ at the cell membrane (Hickman et al., 1994; Humphreys and Dubyak, 1996, 1998; Gudipaty et al., 2001). In the latter paper, surface protein levels as determined by FACS analysis directly correlated with pore formation as measured by uptake of ethidium bromide (M_r = 314). Differences in $P2X_7R$ expression level between different types of lymphocytes also translated into differences in dye uptake (Gu et al., 2000). Furthermore, all cell types had abundant intracellular receptor stores, suggesting regulation of receptor function and pore formation at the level of protein trafficking. We now also demonstrate a cytokine-driven increase in $P2X_7R$ expression at the cell membrane, which in turn correlates with dye uptake. The ability of BzATP to form pores in these cytokine-treated astrocytes would, therefore, be consistent with this “critical density” hypothesis of $P2X_7R$ on the cell membrane for pore formation to occur.

However, in cells of nonhematopoietic lineage, pore formation has not been so consistently observed and only increases in $[Ca^{2+}]_i$ are detected. So, for example, only slightly permeant pores, or none at all develop in human fibroblasts, osteoblasts and Mueller cells in response to ligand binding to $P2X_7R$ (Solini et al., 1999; Nakamura et al., 2000; Pannicke et al., 2000). Cloned $P2X_7R$’s form large pores in HEK cells (Surprenant et al., 1996; Virginio et al., 1999a), but none at all in *Xenopus* oocytes (Klapperstuck et al., 2000). Human B cells also possess pores of limited permeability that take up YO-PRO-1, but not PI (Markwardt et al., 1997; Gu et al., 2000; Lohn et al., 2001). The data for resting human astrocytes are consistent

with this functional profile of the $P2X_7R$, and suggest that IL-1β induces a change in the cellular localization of the $P2X_7R$, as well as an increase of receptor activity.

The detection of the $P2X_7R$ at the cell membrane in human fetal astrocytes adds to a growing literature defining a functional role for this receptor in these cells (Kukley et al., 2001; Panenka et al., 2001; Duan et al., 2003; Gendron et al., 2003a; Nobile et al., 2003). In astrocytes, binding of BzATP has been linked to several cell-signaling pathways including ERK1 and 2 and p38 MAP kinase (Gendron et al., 2003b), as well as the transcriptional complexes AP-1 (Panenka et al., 2001) and NF-κB (Ferrari et al., 1997). BzATP has also been shown to enhance IL-1β-induced activation of NF-κB and AP-1 (John et al., 2001; Panenka et al., 2001). Functionally, the $P2X_7R$ has been linked in mouse astrocytes to the release of the excitatory amino acids L-glutamate and D-aspartate (Duan et al., 2003), as well as to the upregulation of the chemokines MCP-1 and IL-8 in human and rat astrocytes, respectively (John et al., 2001; Panenka et al., 2001). The data presented here show a role for the $P2X_7R$ in upregulation of IL-1β-induced nitric oxide synthase expression. This contributory role of the $P2X_7R$ in proinflammatory gene expression implicates this receptor in a wide range of pathologic conditions of an inflammatory nature. Consistent with this conclusion are the observations that increased expression of the $P2X_7R$ has been observed in the central nervous system of rats in association with necrosis induced by occlusion of the middle cerebral artery (Collo et al., 1997), with plaques in a mouse model of Alzheimer's disease (Parvathenani et al., 2003), and in Mueller cells from patients with proliferative vitreopathy (Bringmann et al., 2002). Our data add to this list, showing that reactive astrocytes associated with MS lesions can be immunostained with an antibody specific for the $P2X_7R$.

The coexpression of multiple metabotropic and ionotropic P2 receptor subtypes in the same cell has been noted in several other cell types (reviewed in Dubyak, 1999), and, at least in some cases, reflects differences in the distribution of these receptors between different polarized compartments of the cell (see, e.g., Luo et al., 1999). This expression of multiple P2 receptor subtypes may, therefore, reflect a requirement for responses to the different ligand affinities of each receptor subtype at these sites. Under normal conditions, the relative agonist potency of ATP at $P2Y_1$ and $P2X_7R$ would be expected to favor $P2Y_1$. Nevertheless, agonist potencies for $P2X_7R$ also suggest a more subtle form of regulating the receptor function by the ionic milieu, since it has been shown that decreased extracellular sodium and chloride ions change the potency of ATP to resemble that of BzATP in monocytes (North and Surprenant, 2000; Gudipaty et al., 2001). Similar results were seen at recombinant receptors, with a 19-fold increase in ATP potency in the absence of sodium chloride (Michel et al., 1999). These modulations of agonist effect act as an additional layer of receptor function regulation. First, the availability of extracellular ATP depends on its release by cell lysis or regulated export from sources such as platelets and neurons (reviewed in Burnstock and Williams, 2000). Second, expression of $P2X_7R$ is regulated by the presence or absence of differentiation cues, such as the cytokines IL-1β or TNF-α. Low levels of $P2X_7R$ expression in resting cells ensures that a small cationic flux occurs in response to agonist binding. Once surface expression has been enhanced, cell-specific factors determine the size and existence of the pores formed. While the levels of ATP in a normal extracellular environment would be expected to provide little stimulus for $P2X_7R$, perturbations of extracellular ionic content will increase ATP potency and receptor activation. Such fluctuations in the local ionic environment might occur following lysis of adjacent cells. Additionally, ischemia can induce the collapse of ionic gradients. At every step, $P2X_7R$ activation would be expected to be carefully fine-tuned according to the presence or absence of inflammatory stimuli and the extracellular ionic environment. Given the properties of $P2X_7R$ and its ability to affect other signaling pathways, such multi-layered regulation would prevent the inappropriate activation of this multifaceted receptor.

ACKNOWLEDGMENTS

This work was supported by USPHS grants NS40137 (to C.F.B.), NS11920 (to C.F.B.), and NS41023 (to E.S.), and by MSTP training grant T32GM07288. The authors thank Wa Shen for culture preparation. We also thank Dr. Gary Buell for providing the monoclonal antibody to $P2X_7R$ and Dr Peter Davies for the monoclonal antibody to NF68.

Grant sponsor: United States Public Health Service; Grant number: NS40137; Grant number:NS11920; Grant number:NS41023; Grant sponsor: MSTP; Grant number:T32GM07288.

REFERENCES

Atkinson L, Milligan CJ, Buckley NJ, Deuchars J. An ATP-gated ion channel at the cell nucleus. Nature 2002;420:42. [PubMed: 12422208]

Berchtold S, Ogilvie AL, Bogdan C, Muhl-Zurbes P, Ogilvie A, Schuler G, Steinkasserer A. Human monocyte derived dendritic cells express functional P2X and P2Y receptors as well as ecto-nucleotidases. FEBS Lett 1999;458:424–428. [PubMed: 10570953]

Bianchi BR, Lynch KJ, Touma E, Niforatos W, Burgard EC, Alexander KM, Park HS, Yu H, Metzger R, Kowaluk E, Jarvis MF, van Biesen T. Pharmacological characterization of recombinant human and rat P2X receptor subtypes. Eur J Pharmacol 1999;376:127–138. [PubMed: 10440098]

Bo X, Jiang LH, Wilson HL, Kim M, Burnstock G, Surprenant A, North RA. Pharmacological and biophysical properties of the human P2X5 receptor. Mol Pharmacol 2003;63:1407–1416. [PubMed: 12761352]

Bringmann A, Pannicke T, Uhlmann S, Kohen L, Wiedemann P, Reichenbach A. Membrane conductance of Muller glial cells in proliferative diabetic retinopathy. Can J Ophthalmol 2002;37:221–227. [PubMed: 12095095]

Buell G, Chessell IP, Michel AD, Collo G, Salazzo M, Herren S, Gretener D, Grahames C, Kaur R, Kosco-Vilbois MH, Humphrey PP. Blockade of human $P2X_7$ receptor function with a monoclonal antibody. Blood 1998;92:3521–3528. [PubMed: 9808543]

Burnstock G, Williams M. P2 purinergic receptors: modulation of cell function and therapeutic potential. J Pharmacol Exp Ther 2000;295:862–869. [PubMed: 11082418]

Chow SC, Kass GE, Orrenius S. Purines and their roles in apoptosis. Neuropharmacology 1997;36:1149–1156. [PubMed: 9364470]

Collo G, Neidhart S, Kawashima E, Kosco-Vilbois M, North RA, Buell G. Tissue distribution of the $P2X_7$ receptor. Neuropharmacology 1997;36:1277–1283. [PubMed: 9364482]

Colomar A, Amedee T. ATP stimulation of $P2X_7$ receptors activates three different ionic conductances on cultured mouse Schwann cells. Eur J Neurosci 2001;14:927–936. [PubMed: 11595031]

Deuchars SA, Atkinson L, Brooke RE, Musa H, Milligan CJ, Batten TF, Buckley NJ, Parson SH, Deuchars J. Neuronal $P2X_7$ receptors are targeted to presynaptic terminals in the central and peripheral nervous systems. J Neurosci 2001;21:7143–7152. [PubMed: 11549725]

Di Virgilio F. The P2Z purinoceptor: an intriguing role in immunity, inflammation and cell death. Immunol Today 1995;16:524–528. [PubMed: 7495489]

Duan S, Anderson CM, Keung EC, Chen Y, Swanson RA. $P2X_7$ receptor-mediated release of excitatory amino acids from astrocytes. J Neurosci 2003;23:1320–1328. [PubMed: 12598620]

Dubyak GR. Focus on “multiple functional P2X and P2Y receptors in the luminal and basolateral membranes of pancreatic duct cells.”. Am J Physiol 1999;277:C202–204. [PubMed: 10444395]

Falzoni S, Munerati M, Ferrari D, Spisani S, Moretti S, Di Virgilio F. The purinergic P2Z receptor of human macrophage cells. Characterization and possible physiological role. J Clin Invest 1995;95:1207–1216. [PubMed: 7883969]

Faneyte IF, Kristel PMP, van de Vijver MJ. Determining MDR1/P-glycoprotein expression in breast cancer. Int J Cancer 2001;93:114–122. [PubMed: 11391630]

Ferrari D, Wesselborg S, Bauer MK, Schulze-Osthoff K. Extracellular ATP activates transcription factor NF-kappaB through the P2Z purinoreceptor by selectively targeting NF-kappaB p65. J Cell Biol 1997;139:1635–1643. [PubMed: 9412459]

Gargett CE, Wiley JS. The isoquinoline derivative KN-62 a potent antagonist of the P2Z-receptor of human lymphocytes. Br J Pharmacol 1997;120:1483–1490. [PubMed: 9113369]

Gendron FP, Neary JT, Theiss PM, Sun GY, Gonzalez FA, Weisman GA. Mechanisms of $P2X_7$ receptor-mediated ERK1/2 phosphorylation in human astrocytoma cells. Am J Physiol Cell Physiol 2003a; 284:C571–581. [PubMed: 12529254]

Gendron F-P, Chalimoniuk M, Strosznajder J, Shen S, Gonzalez FA, Weisman GA, Sun GY. $P2X_7$ nucleotide receptor activation enhances IFNγ-induced type II nitric oxide synthase activity in BV-2 microglial cells. J Neurochem 2003b;87:344–352. [PubMed: 14511112]

Grynkiewicz G, Poenie M, Tsien RY. A new generation of Ca^{2+} indicators with greatly improved fluorescence properties. J Biol Chem 1985;260:3440–3450. [PubMed: 3838314]

Gu BJ, Zhang WY, Bendall LJ, Chessell IP, Buell GN, Wiley JS. Expression of $P2X_7$ purinoceptors on human lymphocytes and monocytes: evidence for nonfunctional $P2X_7$ receptors. Am J Physiol Cell Physiol 2000;279:C1189–1197. [PubMed: 11003599]

Gu BJ, Zhang W, Worthington RA, Sluyter R, Dao-Ung P, Petrou S, Barden JA, Wiley JS. A Glu-496 to Ala polymorphism leads to loss of function of the human $P2X_7$ receptor. J Biol Chem 2001;276:11135–11142. [PubMed: 11150303]

Gudipaty L, Humphreys BD, Buell G, Dubyak GR. Regulation of $P2X_7$ nucleotide receptor function in human monocytes by extracellular ions and receptor density. Am J Physiol Cell Physiol 2001;280:C943–953. [PubMed: 11245611]

Gudipaty L, Munetz J, Verhoef PA, Dubyak GR. Essential role for Ca^{2+} in regulation of IL-1{beta} secretion by $P2X_7$ nucleotide receptor in monocytes, macrophages, and HEK-293 cells. Am J Physiol Cell Physiol 2003;285:C286–299. [PubMed: 12660148]

Hickman S, el Khoury J, Greenberg S, Schieren I, Silverstein S. P2Z adenosine triphosphate receptor activity in cultured human monocyte-derived macrophages. Blood 1994;84:2452–2456. [PubMed: 7919365]

Hu Y, Fisette PL, Denlinger LC, Guadarrama AG, Sommer JA, Proctor RA, Bertics PJ. Purinergic receptor modulation of lipopolysaccharide signaling and inducible nitric-oxide synthase expression in RAW 264.7 macrophages. J Biol Chem 1998;273:27170–27175. [PubMed: 9765236]

Humphreys BD, Dubyak GR. Induction of the P2z/$P2X_7$ nucleotide receptor and associated phospholipase D activity by lipopolysaccharide and IFN-gamma in the human THP-1 monocytic cell line. J Immunol 1996;157:5627–5637. [PubMed: 8955215]

Humphreys BD, Dubyak GR. Modulation of $P2X_7$ nucleotide receptor expression by pro- and anti-inflammatory stimuli in THP-1 monocytes. J Leukoc Biol 1998;64:265–273. [PubMed: 9715267]

Humphreys BD, Virginio C, Surprenant A, Rice J, Dubyak GR. Isoquinolines as antagonists of the $P2X_7$ nucleotide receptor: high selectivity for the human versus rat receptor homologues. Mol Pharmacol 1998;54:22–32. [PubMed: 9658186]

John GR, Simpson JE, Woodroofe MN, Lee SC, Brosnan CF. Extracellular nucleotides differentially regulate interleukin-1beta signaling in primary human astrocytes: implications for inflamma-tory gene expression. J Neurosci 2001;21:4134–4142. [PubMed: 11404398]

Jones CA, Chessell IP, Simon J, Barnard EA, Miller KJ, Michel AD, Humphrey PP. Functional characterization of the $P2X_4$ receptor orthologues. Br J Pharmacol 2000;129:388–394. [PubMed: 10694247]

Kim M, Jiang LH, Wilson HL, North RA, Surprenant A. Proteomic and functional evidence for a $P2X_7$ receptor signalling complex. EMBO J 2001;20:6347–6358. [PubMed: 11707406]

Klapperstuck M, Buttner C, Bohm T, Schmalzing G, Markwardt F. Characteristics of $P2X_7$ receptors from human B lymphocytes expressed in *Xenopus* oocytes. Biochim Biophys Acta 2000;1467:444–456. [PubMed: 11030601]

Kukley M, Barden JA, Steinhauser C, Jabs R. Distribution of P2X receptors on astrocytes in juvenile rat hippocampus. Glia 2001;36:11–21. [PubMed: 11571780]

Laliberte R, Perregaux D, Svensson L, Pazoles CJ, Gabel CA. Tenidap modulates cytoplasmic pH and inhibits anion transport in vitro. II. Inhibition of IL-1 beta production from ATP-treated monocytes and macrophages. J Immunol 1994;153:2168–2179. [PubMed: 8051418]

Lee SC, Liu W, Brosnan CF, Dickson DW. Characterization of primary human fetal dissociated central nervous system cultures with an emphasis on microglia. Lab Invest 1992;67:465–476. [PubMed: 1359193]

Lee SC, Dickson DW, Liu W, Brosnan CF. Induction of nitric oxide synthase activity in human astrocytes by interleukin-1 beta and interferon-gamma. J Neuroimmunol 1993;46:19–24. [PubMed: 7689587]

Lee SC, Liu W, Dickson DW, Brosnan CF. In human fetal astrocytes exposure to interleukin-1 beta stimulates acquisition of the GD3+ phenotype and inhibits cell division. J Neurochem 1995;64:1800–1807. [PubMed: 7891108]

Liu JS, Zhao ML, Brosnan CF, Lee SC. Expression of inducible nitric oxide synthase and nitrotyrosine in multiple sclerosis lesions. Am J Pathol 2001;158:2057–2066. [PubMed: 11395383]

Liu JS, John GR, Sikora A, Lee SC, Brosnan CF. Modulation of interleukin-1beta and tumor necrosis factor alpha signaling by P2 purinergic receptors in human fetal astrocytes. J Neurosci 2000;20:5292–5299. [PubMed: 10884313]

Lohn M, Klapperstuck M, Riemann D, Markwardt F. Sodium block and depolarization diminish P2Z-dependent Ca^{2+} entry in human B lymphocytes. Cell Calcium 2001;29:395–408. [PubMed: 11352505]

Luo X, Zheng W, Yan M, Lee MG, Muallem S. Multiple functional P2X and P2Y receptors in the luminal and basolateral membranes of pancreatic duct cells. Am J Physiol 1999;277:C205–215. [PubMed: 10444396]

MacKenzie A, Wilson HL, Kiss-Toth E, Dower SK, North RA, Surprenant A. Rapid secretion of interleukin-1beta by microvesicle shedding. Immunity 2001;15:825–835. [PubMed: 11728343]

Markwardt F, Lohn M, Bohm T, Klapperstuck M. Purinoceptor-operated cationic channels in human B lymphocytes. J Physiol 1997;498(Pt 1):143–151. [PubMed: 9023774]

Mensink E, van de Locht A, Schattenberg A, Linders E, Schaap N, Geurts van Kessel A, De Witte T. Quantitation of minimal residual disease in Philadelphia chromosome positive chronic myeloid leukaemia patients using real-time quantitative RT-PCR. Br J Haematol 1998;102:768–774. [PubMed: 9722305]

Michel AD, Chessell IP, Humphrey PP. Ionic effects on human recombinant $P2X_7$ receptor function. Naunyn Schmiedebergs Arch Pharmacol 1999;359:102–109. [PubMed: 10048594]

Nakamura E, Uezono Y, Narusawa K, Shibuya I, Oishi Y, Tanaka M, Yanagihara N, Nakamura T, Izumi F. ATP activates DNA synthesis by acting on P2X receptors in human osteoblast-like MG-63 cells. Am J Physiol Cell Physiol 2000;279:C510–519. [PubMed: 10913018]

Nobile M, Monaldi I, Alloisio S, Cugnoli C, Ferroni S. ATP-induced, sustained calcium signalling in cultured rat cortical astrocytes: evidence for a non-capacitative, $P2X_7$-like-mediated calcium entry. FEBS Lett 2003;538:71–76. [PubMed: 12633855]

North RA, Surprenant A. Pharmacology of cloned P2X receptors. Annu Rev Pharmacol Toxicol 2000;40:563–580. [PubMed: 10836147]

O'Reilly BA, Kosaka AH, Chang TK, Ford AP, Popert R, Rymer JM, McMahon SB. A quantitative analysis of purinoceptor expression in human fetal and adult bladders. J Urol 2001;165:1730–1734. [PubMed: 11342965]

Panenka W, Jijon H, Herx LM, Armstrong JN, Feighan D, Wei T, Yong VW, Ransohoff RM, MacVicar BA. $P2X_7$-like receptor activation in astrocytes increases chemokine monocyte chemoattractant protein-1 expression via mitogen-activated protein kinase. J Neurosci 2001;21:7135–7142. [PubMed: 11549724]

Pannicke T, Fischer W, Biedermann B, Schadlich H, Grosche J, Faude F, Wiedemann P, Allgaier C, Illes P, Burnstock G, Reichenbach A. $P2X_7$ receptors in Muller glial cells from the human retina. J Neurosci 2000;20:5965–5972. [PubMed: 10934244]

Parvathenani LK, Tertyshnikova S, Greco CR, Roberts SB, Robertson B, Posmantur R. $P2X_7$ mediates superoxide production in primary microglia and is up-regulated in a transgenic mouse model of Alzheimer's disease. J Biol Chem 2003;278:13309–13317. [PubMed: 12551918]

Per Larsson K, Jon Hansen A, Dissing S. The human SH-SY5Y neuroblastoma cell-line expresses a functional $P2X_7$ purinoceptor that modulates voltage-dependent Ca^{2+} channel function. J Neurochem 2002;83:285–298. [PubMed: 12423239]

Raine, C. The lesion in multiple sclerosis and chronic relapsing experimental allergic encephalomyelitis: a structural comparison. In: Raine, CS.; McFarland, HF.; Tourtellotte, WW., editors. Multiple sclerosis: clinical and pathogenetic basis. Chapman & Hall; London: 1997. p. 243-286.

Ramirez AN, Kunze DL. P2X purinergic receptor channel expression and function in bovine aortic endothelium. Am J Physiol Heart Circ Physiol 2002;282:H2106–2116. [PubMed: 12003818]

Rassendren F, Buell GN, Virginio C, Collo G, North RA, Surprenant A. The permeabilizing ATP receptor, $P2X_7$. Cloning and expression of a human cDNA. J Biol Chem 1997;272:5482–5486. [PubMed: 9038151]

Scemes E, Suadicani SO, Spray DC. Intercellular communication in spinal cord astrocytes: fine tuning between gap junctions and P2 nucleotide receptors in calcium wave propagation. J Neurosci 2000;20:1435–1445. [PubMed: 10662834]

Smart ML, Gu B, Panchal RG, Wiley J, Cromer B, Williams DA, Petrou S. $P2X_7$ receptor cell surface expression and cytolytic pore formation are regulated by a distal C-terminal region. J Biol Chem 2003;278:8853–8860. [PubMed: 12496266]

Solini A, Chiozzi P, Morelli A, Fellin R, Di Virgilio F. Human primary fibroblasts in vitro express a purinergic $P2X_7$ receptor coupled to ion fluxes, microvesicle formation and IL-6 release. J Cell Sci 1999;112:297–305. [PubMed: 9885283]

Solle M, Labasi J, Perregaux DG, Stam E, Petrushova N, Koller BH, Griffiths RJ, Gabel CA. Altered cytokine production in mice lacking $P2X_7$ receptors. J Biol Chem 2001;276:125–132. [PubMed: 11016935]

Steinberg TH, Newman AS, Swanson JA, Silverstein SC. ATP4-permeabilizes the plasma membrane of mouse macrophages to fluorescent dyes. J Biol Chem 1987;262:8884–8888. [PubMed: 3597398]

Surprenant A, Rassendren F, Kawashima E, North RA, Buell G. The cytolytic P2Z receptor for extracellular ATP identified as a P2X receptor ($P2X_7$). Science 1996;272:735–738. [PubMed: 8614837]

Virginio C, MacKenzie A, North RA, Surprenant A. Kinetics of cell lysis, dye uptake and permeability changes in cells expressing the rat $P2X_7$ receptor. J Physiol 1999a;519(Pt2):335–346. [PubMed: 10457053]

Virginio C, MacKenzie A, Rassendren FA, North RA, Surprenant A. Pore dilation of neuronal P2X receptor channels. Nat Neurosci 1999b;2:315–321. [PubMed: 10204537]

Wiley JS, Gargett CE, Zhang W, Snook MB, Jamieson GP. Partial agonists and antagonists reveal a second permeability state of human lymphocyte P2Z/$P2X_7$ channel. Am J Physiol 1998;275:C1224–1231. [PubMed: 9814970]

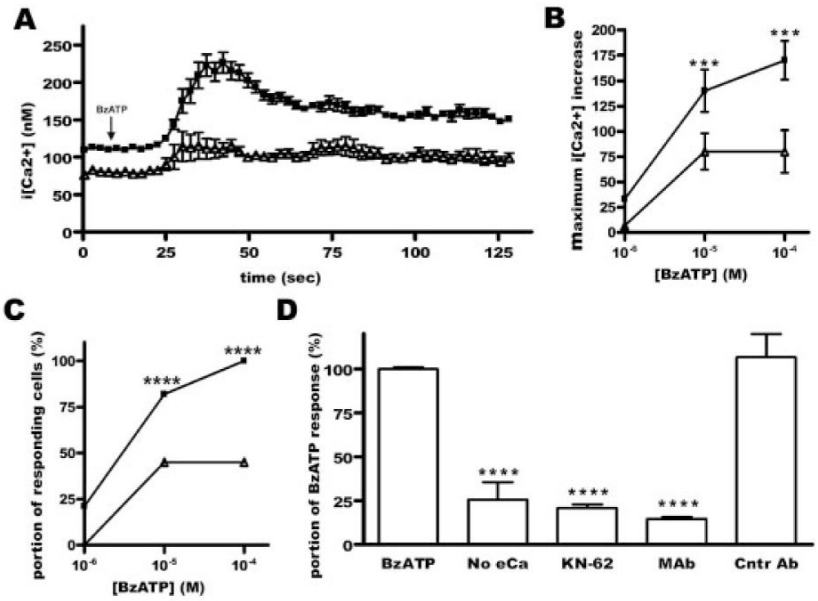

Fig. 1.

IL-1β increases the astrocytic calcium response to BzATP. Human fetal astrocytes were activated with 10 ng/ml IL-1β for 24 h (closed squares) or subjected to a medium change as a control (open triangles). They were then loaded with Fura-2 for 45 min and fluctuations in $[Ca^{2+}]_i$ (nM) determined as described in Methods. **A:** Changes in intracellular calcium levels over time following application of 100 μM BzATP. **B:** Cells were treated with indicated doses of BzATP and changes in intracellular calcium determined. Calcium increases are expressed as the maximal increase in intracellular calcium (nM) over baseline ±SEM, $P < 0.001$ (***) by two-way ANOVA comparing treatment and dose. **C:** Cells were treated with indicated doses of BzATP and the percentage of cells responding with an increase in intracellular calcium ≥40 nM determined. A—C: Representative of astrocytes collected from three different brains, showing data from > 30 cells per treatment, ±SEM where applicable. **D:** The absence of extracellular calcium (eCa), pretreatment with 10 nM KN-62, or the addition of a blocking monoclonal antibody (MAb) or irrelevant isotype control antibody (Cntr Ab) on the BzATP-induced increase in intracellular calcium in IL-1β-activated astrocytes is shown. The value for the first bar in D is 170 nM ± 19 $[Ca^{2+}]_i$. Data are expressed as percentage change from the response to BzATP alone and represent pooled data from four different experiments ±SEM. $P < 0.0001$ (****) vs. BzATP alone by one-way ANOVA followed by Dunnett's multiple comparison test for all groups except the isotype control group, which was not significantly different.

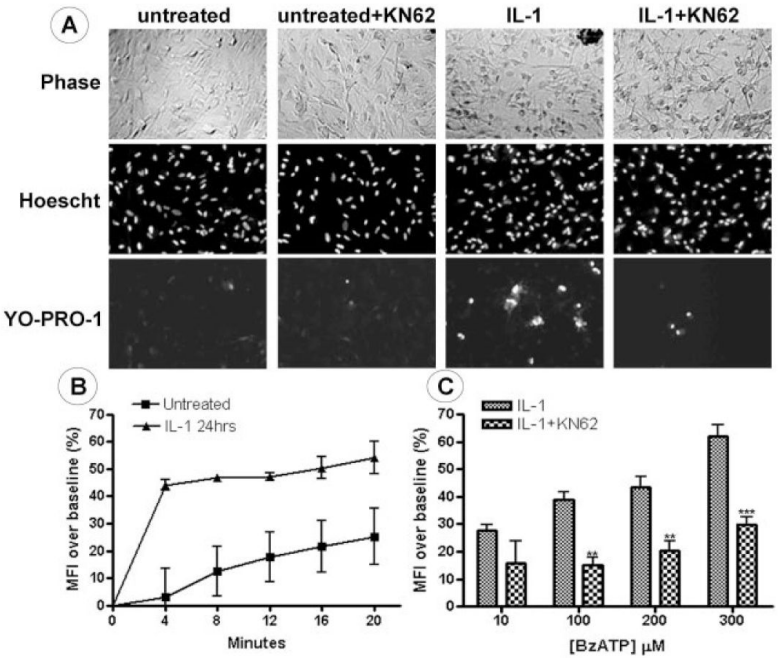

Fig. 2.

YO-PRO-1 uptake is enhanced by IL-1β. **A:** Membrane pore formation was determined by uptake of the fluorescent dye YO-PRO-1 as described in Methods. Matched phase (upper), Hoescht (middle), and YO-PRO-1 (lower) are shown. Left to right: control untreated astrocytes, control cells pretreated with KN-62, astrocytes activated with IL-1β for 24 h, and activated cells pretreated with KN-62, 40×. All photographs were taken 10 min after addition of 100μM BzATP. Representative data from four separate experiments utilizing cells from four different brains are shown. **B:** Spectrophotometric measurement of YO-PRO-1 uptake in astrocytes treated with 10 ng/ml IL-1β for 24 h (triangles) or controls (squares) in the presence of 100 μM BzATP. No significant uptake was observed in either the untreated or cytokine-stimulated cells in the absence of BzATP. Data shown represent 12 wells per treatment ±SEM, $P < 0.0001$ (****) for all time points by paired Student's *t*-test. **C:** KN-62 blockade of YO-PRO-1 uptake in response to 10, 100, 200 or 300μM BzATP. Cells were pretreated with 10 nM KN-62. Data shown represent six wells per treatment ±SEM. $P < 0.01$ (**) for 100 and 200 μM, and $P < 0.001$ (***) for μM BzATP by Bonferroni posttest.

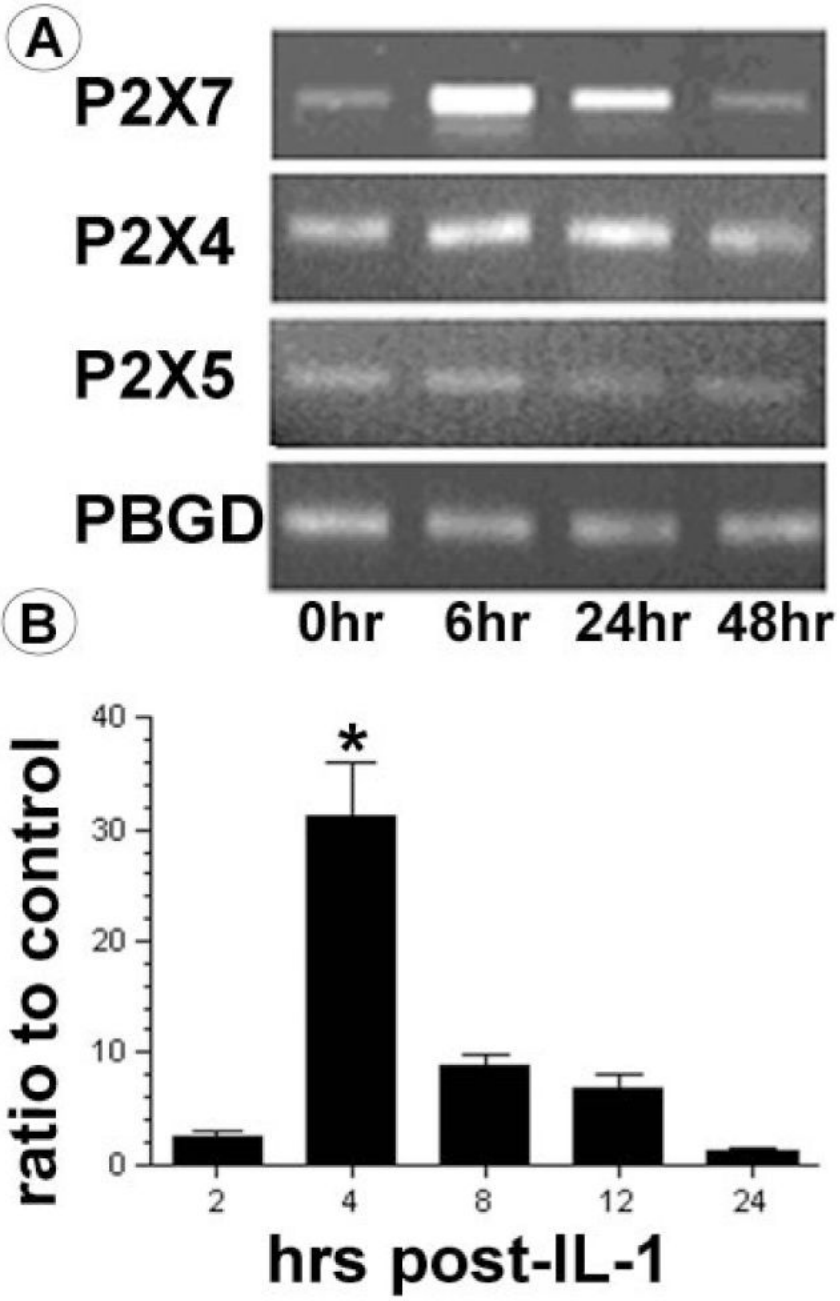

Fig. 3.

IL-1β increases astrocytic expression of $P2X_7R$ mRNA. **A:** RT-PCR analysis of $P2X_7R$ mRNA expression at the indicated hours post-activation with IL-1β. cDNA was analyzed for the presence of $P2X_7R$ (591bp), $P2X_4R$ (426bp), $P2X_5R$ (596 bp) and the control gene, PBGD (337 bp). A $P2X_2R$ transcript (355 bp) was not detected in these cells. **B:** qPCR analysis of IL-1-induced $P2X_7R$ expression, shown as a fold induction above resting levels. Data shown are representative of results from three separate experiments using astrocytes from three different brains, $*P < 0.0001$ to control by one-way ANOVA.

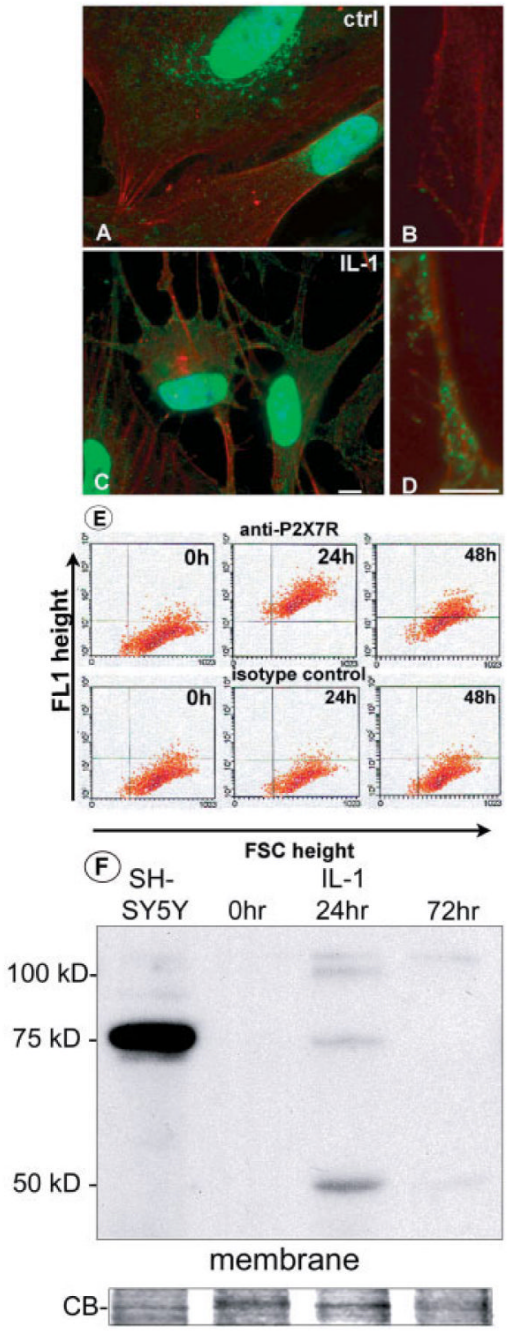

Fig. 4.

IL-1β Increases astrocytic expression of $P2X_7R$ protein as determined by immunohistochemical labeling. **A—D:** Immunofluores-cent images of $P2X_7R$ expression by primary astrocytes in culture. $P2X_7R$ expression was detected using a rabbit polyclonal antibody and an Alexa 488-coupled secondary antibody (green). Actin filaments were stained with rhodamine phalloidin (red) and nuclei visualized with DAPI (blue). A,B: Untreated control astrocytes and panels C and D astrocytes treated with IL-1β for 24 h. Distance marker represents 10 μM. **E:** FACS analysis of astrocytes at 0 h, 24 h, and 48 h after treatment with 10 ng/ml IL-1β and immunostained for $P2X_7R$ (upper) or an isotype-matched control antibody (lower) and a secondary antibody coupled to FITC (FL1). Cells (10,000 per sample) were gated

on the living cell population, as determined by exclusion of PI reactivity. Data shown represent results from three independent experiments using astrocytes from different brains. **F:** Astrocyte samples were left untreated (0 h) or treated with IL-1β for 24 and 72 h and cell lysates subjected to fractionation to provide membrane fractions as described in Methods. Membrane preparations from untreated SH-SY5Y cells were collected in parallel. Western blotting was carried out with the polyclonal $P2X_7R$-specific antibody. Coomassie blue (CB) images are shown beneath each blot as a loading control. Data shown are representative of three independent experiments.

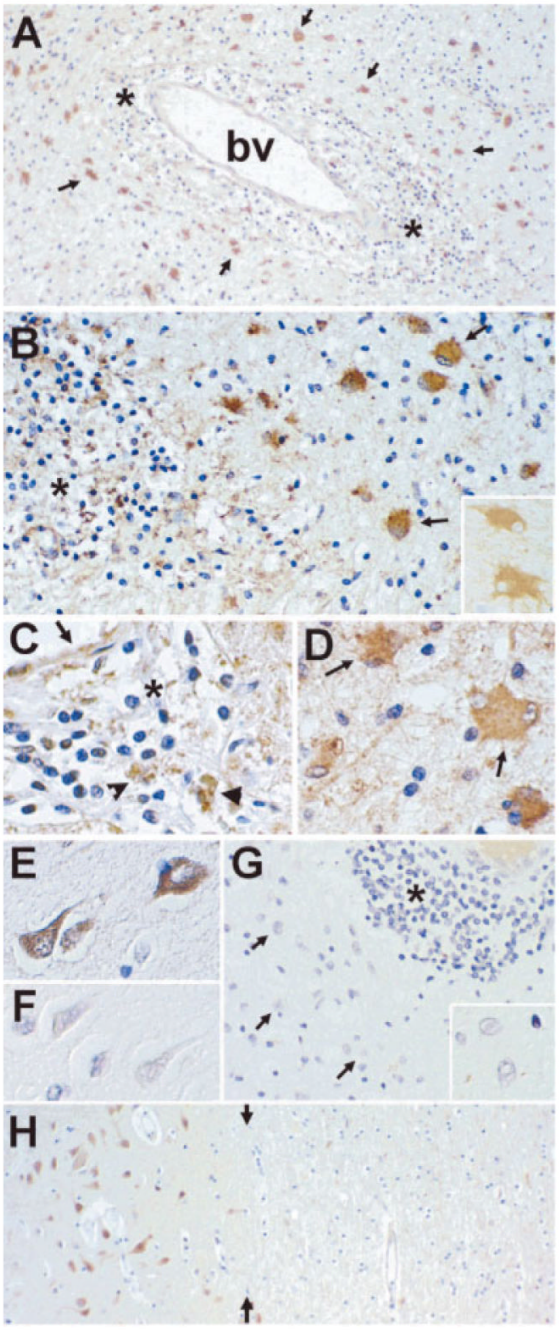

Fig. 5.

Immunoreactivity for the $P2X_7R$ in multiple sclerosis tissues. **A:** Low-power view of an inflamed vessel (bv) in a chronic active multiple sclerosis lesion showing the diffuse distribution of $P2X_7R$+ cells (brown). $P2X_7R$ immunoreactivity was detected in association with cells in the perivascular infiltrates (asterisk) as well as with hypertrophic astrocytes (arrows) in the surrounding parenchyma. **B:** Higher-power view of the inflammatory infiltrate and surrounding parenchymal tissue from the same lesion illustrated in A. Inset shows a parallel section immunoreacted with an antibody to GFAP to identify astrocytes. **C:** High-power view of the inflammatory infiltrate surrounding another vessel. $P2X_7R$ immunoreactivity was detected on cells within the inflammatory infiltrate (arrowheads) as well as on the endothelial

cells (arrow). **D:** High-power view of $P2X_7R$+ hypertrophic astrocytes. **E:** High-power view of $P2X_7R$+ neurons. **F:** High-power view of a similar area to (E) that had been reacted with the polyclonal $P2X_7R$ antibody adsorbed with specific peptide. **G:** Low-power view of the edge of an inflamed vessel reacted with the $P2X_7R$ antibody adsorbed with specific peptide. Inset shows high-power view of a hypertrophic astrocyte. **H:** Low-power view of the gray-white matter border (marked with arrows) in a noninflamed area of the same brain shown in A. $P2X_7R$+ neurons are visible in the gray matter area (left of image), whereas only a low-level immunoreactivity for the $P2X_7R$is found in the adjacent white matter (right of image). All sections were counterstained with hematoxylin. A, ×60; B, ×120 (inset ×240); C-F, ×240; G, ×100 (inset ×240); H, ×60.

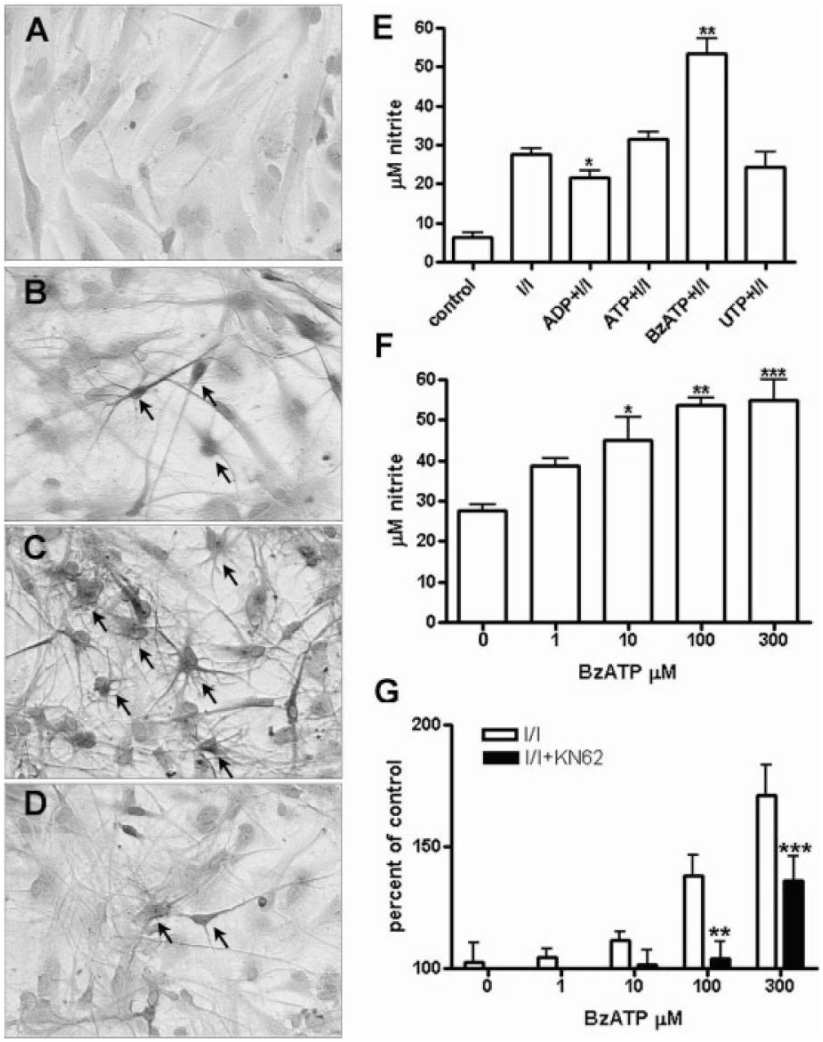

Fig. 6.

BzATP enhances NO production induced by IL-1β plus IFNγ. Expression of NOS2 in astrocytes was induced by activation with 10 ng/ml IL-1β and IFNγ (I/I) for 72h. **A—D:** Immunohistochemical analysis of NOS2 immunoreactivity in (A) resting astrocytes, (B) cells treated for 72 h with I/I alone, (C) cells co-treated with 100 BzATP, or (D) cells pretreated with 10 nM KN-62 before BzATP and cytokine addition. **E:** Cells were treated with P2 receptor agonists as shown and nitrite concentrations determined using the Griess reagent. Statistical analysis revealed no significance except for $P < 0.01$ (**) for BzATP compared with I/I alone and $P < 0.05$ (*) for ADP compared with I/I alone by Dunnett's multiple comparison test. **F:** Cells were treated with increasing doses of BzATP as shown and nitrite concentrations determined as above. Statistical analysis revealed increasing significance with increasing dose, $P < 0.05$ (*), 0.01 (**) and 0.001 (***) for 10, 100, and 300 μM, respectively, by one-way ANOVA. **G:** Cells were treated with I/I and varying BzATP doses with or without 10 nM KN-62 pretreatment for 72 h and nitrite concentrations determined. Data are shown as a percentage of I/I alone. BzATP effects were diminished by KN-62 pretreatment for 100 and 300 μM BzATP, $P < 0.05$ (*) and $P < 0.01$ (**) by Bonferroni post test (pooled data from three cases, six wells per case).